Journal of Molecular Spectroscopy 348 (2018) 142–151

Contents lists available at ScienceDirect

Journal of Molecular Spectroscopy

journal homepage: www.elsevier.com/locate/jms

Laser absorption spectroscopy applied to monitoring of short-lived climate pollutants (SLCPs)

Gaoxuan Wang [a], Fengjiao Shen [a], Hongming Yi [a,1], Patrice Hubert [b], Alexandre Deguine [b], Denis Petitprez [b], Rabih Maamary [a,2], Patrick Augustin [a], Marc Fourmentin [a], Eric Fertein [a], Markus W. Sigrist [c], Tong-Nguyen Ba [a], Weidong Chen [a,*]

[a] Laboratoire de Physicochimie de l'Atmosphère, Université du Littoral Côte d'Opale, Dunkerque, France
[b] Physicochimie des Processus de Combustion et de l'Atmosphère, Université de Lille 1, Villeneuve d'Ascq, France
[c] Laser Spectroscopy and Sensing Laboratory, IQE-ETH Zurich, Zurich, Switzerland

ARTICLE INFO

Article history:
Received 25 September 2017
In revised form 29 March 2018
Accepted 29 March 2018
Available online 30 March 2018

ABSTRACT

Enhanced mitigation of short-lived climate pollutants (SLCPs) has been recently paid more attention in order to provide more sizeable short-term reductions of global warming effects over the next several decades. We overview in this article our recent progress in the development of spectroscopic instruments for optical monitoring of major SLCPs based on laser absorption spectroscopy. Methane (CH_4) and black carbon (BC) are the most important SLCPs contributing to the human enhancement of the global greenhouse effect after CO_2. We present optical sensing of these two climate-change related atmospheric species to illustrate how "classical" spectroscopy can help to address today's challenging issues: (1) Photoacoustic measurements of BC optical absorption coefficient in order to determine its radiative-forcing related optical parameters (such as mass absorption coefficient, absorption Ångström coefficient) with higher precision (~7.4% compared to 12–30% for filter-based methods routinely used nowadays). The 1σ (SNR = 1) minimum measurable volumetric mass density of 21 ng/m^3 (in 60 s) for black carbon. (2) Direct absorption spectroscopy-based monitoring of methane (CH_4) in field campaign to identify pollution source in conjunction with air mass back-trajectory modeling. Using a White-type multipass cell (an effective path-length of 175 m), a 1σ detection limit of 33.3 ppb in 218 s was achieved with a relative measurement precision of 1.1% and an overall measurement uncertainty of about 5.1%.

Performance of the custom, lab-based instruments (in terms of detection limits, measurement precision, temporal response, etc.), spectroscopic measurement aspects, experimental details, spectral data processing, analysis and modeling of the observed environmental episode will be presented and discussed.

© 2018 Elsevier Inc. All rights reserved.

1. Introduction

Global efforts to mitigate climate change have largely focused on reduction of carbon dioxide (CO_2) emissions, which is responsible for 55–60% of current anthropogenic radiative forcing on warming impact. Because of its long lifetime (~130 years [1]) in the atmosphere, long-lasting CO_2 will remain the primary driver of long-term temperature rise even if new CO_2 emissions dropped to zero. A "fast-action" climate mitigation strategy is therefore strongly needed to provide more sizeable short-term benefits than CO_2 reductions. Reduction of emission of short-lived climate pollutants (SLCPs) becomes very important, because they have a significant warming influence on climate with atmospheric lifetimes of less than 20 years [2] which would allow us to quickly lower their concentrations in the atmosphere and hence slow climate change over the next several decades. The main SLCPs are black carbon (BC), methane (CH_4) and tropospheric ozone (O_3), which are the most important contributors to the human enhancement of the global greenhouse effect after CO_2 (see Fig. 1). These SLCPs are also dangerous air pollutants, with various detrimental impacts on human health, agriculture and ecosystems. Monitoring of such climatically and environmentally active SLCPs is important not only for policy-based reporting, but also for basic process-based understanding of climate related processes in the atmosphere.

In this article, we will overview our recent progress in the developments and applications of laser-based spectroscopic instruments for the measurements of climate-change related

* Corresponding author.
E-mail address: chen@univ-littoral.fr (W. Chen).
[1] Now with NIST, Gaithersburg, Maryland, USA.
[2] Now with Université de Reims, France.

https://doi.org/10.1016/j.jms.2018.03.015
0022-2852/© 2018 Elsevier Inc. All rights reserved.

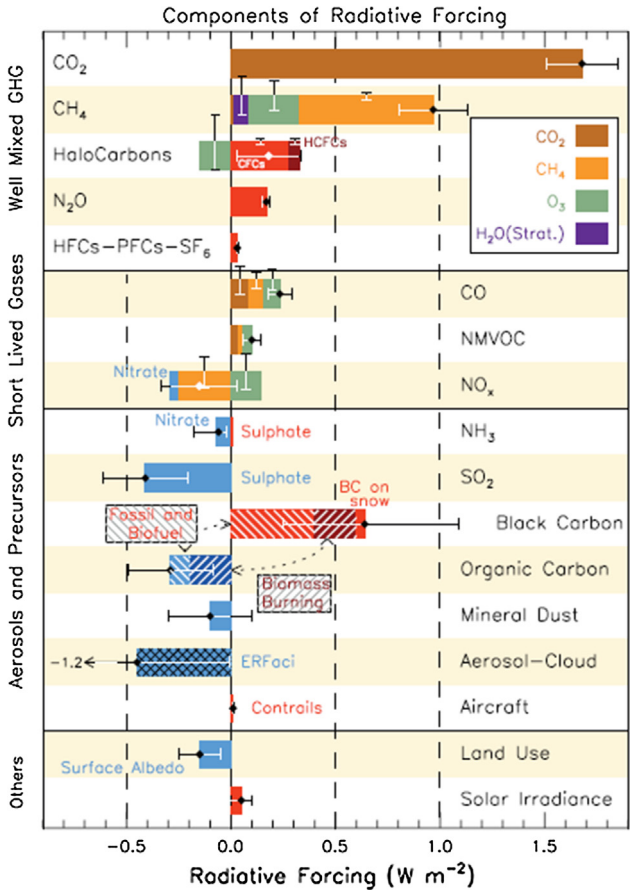

Fig. 1. Main perturbation agents forcing the climate since 1850: CO_2, the single most important agent, associated to other important agents (CH_4, black carbon, tropospheric O_3, etc.) exerting together greater influence than CO_2 [3].

atmospheric SLCPs through two illustrative examples to show how "classical" spectroscopy can help to address today's challenging issues: (1) "classical" photoacoustic spectroscopy (PAS) applied to filter-free measurements of BC optical absorption coefficients, which allowed us to reduce significantly measurement uncertainty in comparison with filter-based routine measurement methods, and (2) direct absorption spectroscopy-based field-monitoring of environmental CH_4 to identify pollution source with the help of the HYSPLIT modeling of air mass back-trajectories.

2. Measurements of BC by photoacoustic spectroscopy (PAS)

Black carbon (BC) is a primary aerosol emitted directly from incomplete combustion processes such as fossil fuel and biomass burning and is characterized by its strong absorption in the visible and near-infrared [4,5]. BC, with an atmospheric lifetime of about one week, is the most important SLCPs [2,3,6]. The uncertainties associated to BC radiative forcing are nowadays still larger than 70%, as shown in Fig. 1, primarily due to the lack of precise knowledge of the optical properties (wavelength-dependent absorption and scattering coefficients) of BC coated with organic aerosol in the atmosphere [5]. In addition, a lack of global scale assessment of BC leads also to high uncertainties in the estimation of its radiative forcing capacity (which reveals the importance of development of cost-effective measurement instrument like PAS sensor as presented in this paper).

For instance, the mass absorption coefficient (MAC) of BC, a fundamental input to models of radiative transfer [5], is determined using filter-based techniques. The filter-based photon-absorption techniques, such as aethalometry and particle soot absorption photometer (PASP) [7], measure the resulting change in light transmittance through filters with aerosols deposit. These techniques do not directly determine the aerosol absorption σ_{abs}, but the attenuation coefficient through the deposit filter σ_{ATN} [7]. During the accumulative process for aerosols, the filter strongly affects the aerosol-light interaction via the effects such as shadowing, multiple and total scattering, and filter loading, which causes the overestimate measurement of absorption with uncertainties of 20–35% [8]. Such large uncertainties may confound our understanding of trends, spatial and temporal variability of BC and its impacts on climate.

BC has been also identified as the most harmful air pollutant in terms of its adverse impacts on human health [9]. Determination of BC mass concentration from the total light absorption resulting from BC and non BC (organic carbon and dust) is another challenging task.

In order to reduce such large uncertainty associated with the indirect measurement methods, photoacoustic (PA) spectrophone is commonly recognized as one of the suitable instruments for direct measurements of aerosol absorption with a uncertainty of <10% [10–12]. In the present work, a microphone-based PA spectrophone was developed for filter-free direct measurement of black carbon's mass absorption coefficient.

PAS technique [13,14] relies on the measurement of photon-absorption induced acoustic signal to infer light absorption information (absorption coefficients, concentrations, etc.) of the target molecules or particles. Gaseous species or aerosol particles irradiated by a light beam modulated at a frequency f_m are heated by light absorption. The heat is transferred to the surrounding medium, which in consequence expands periodically with the modulation of the exciting light (Fig. 2). This thermal expansion results in generation of a pressure wave (hence an acoustic signal) that can be measured using conventional electrets or condenser microphones [15], quartz tuning forks (QTF) [16,17], Cantilever [18], or Micro-electromechanical system (MEMS) microphone [19].

In case of using microphone-based PA spectrophone to measure light absorption by atmospheric species, the PA signal S can be expressed as follows:

$$S = P \times M \times C_{cell} \times \alpha_0 \times C + S_b \quad (1)$$

where S in [V] is the magnitude of the PA signal, P in [W] is the incident exciting light power, M in [V/Pa] is the sensitivity of the used microphone(s). C_{cell} in [Pa m W^{-1}] is the PA absorption cell

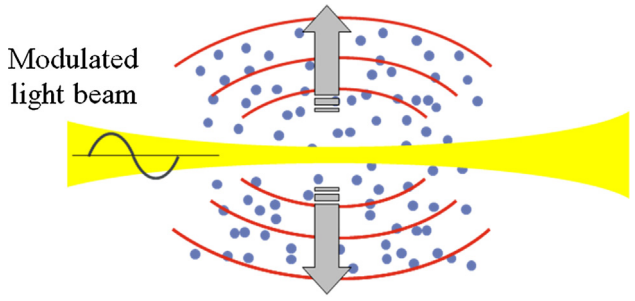

Absorbed energy from the modulated light
=> local heating
=> thermal expansion => pressure wave / sound

Fig. 2. Principle of photoacoustic spectroscopy involving photon-absorption induced acoustic signal: the absorbed energy from light produces local heating and then generates a pressure wave (sound) through thermal expansion.

constant. S_b (V) is the background PA noise. In case of aerosol particle measurement, α_0 is the aerosol MAC (mass absorption coefficient) in [$m^{-1}/(\mu g/m^3)$] and C is the aerosol mass concentration in [$\mu g/m^3$].

PAS technique offers a unique advantage over other spectroscopic methods: the PA signal increases with the exciting optical light power. In contrast to other spectroscopic techniques involving a voluminous light–gas interaction module (like multipass cell, cavity, open path, etc.) and expensive wavelength-dependent photodetector, PAS-based sensors allows high-sensitivity measurements in a very small gas sample volume (of a few cm^3 or less) with a high dynamic measurement range of 6–9 orders of magnitude because of the large dynamic range of common acoustic transducer responsivity. Moreover, the acoustic transducers (microphone, QTF, etc.) are truly cost-effective, and their responsivity is wavelength-independent.

PA measurement technique is very suitable for applications in harsh environment (advantageous over cavity enhanced setups where protecting the high-reflectivity cavity mirrors against contamination by dust is always a serious issue to be addressed).

2.1. Photoacoustic spectrophone – experimental setup

The PAS-based optical sensor used in the present work is schematically presented in Fig. 3. The light source used was a high power blue laser diode operating at 444 nm with a FWHM (full width at half maximum) of 1 nm. The maximum laser output power was ~1 W powered with a diode current of 1 A and a drive voltage of 5 V by means of a diode laser controller (Arryo instrument 6340). Electret condenser microphones (EK-23329-P07) were used as acoustic transducer for acoustic signal measurement.

A single-pass longitudinal photoacoustic resonator was used as PA cell. It consisted of a 26 mm long cylinder with a diameter of 6 mm. The PA cell was sealed with UV fused silica windows (transmission of >90%). A buffer volume at each extreme side of the PA cell was designed to remove thermal noise resulting from absorption of incident laser intensity by the PA cell's windows. The PA cell had a Q-factor of about 8.

A mechanical chopper (SR540, Stanford Res. Inc.) was used for modulation of the laser intensity at 6260 Hz to match the eigen resonant frequency of the longitudinal acoustic mode of the used cylindrical PA cell to enhance the photoacoustic signal. A power meter (Coherent, FieldMasterTM GS) was used to monitor the laser diode power through the PA cell.

Acoustic signal from microphones was pre-amplified first and then feeded to a lock-in amplifier (SR830, Stanford Res. Inc.) for demodulation of the modulated PA signal at the light modulation frequency. A laptop was used to control, via a Labview software, the measurement and the data acquisition using a National Instrument PCI-6251 card (16-Bit with a sampling rate of 1 MS/s for multichannel and 1.25 MS/s for 1-Channel), to perform data processing and to display the measurement results.

2.2. Calibration of the PA spectrophone

As shown in Eq. (1), once the PA cell constant C_{cell} is known, the aerosol MAC α_0 (in [$m^{-1}/(\mu g/m^3)$]) can be determined from the experimentally measured PA signal amplitudes S (in [V]) and the background PA noise S_b (in [V]), the incident light power P (in [W]), in association with the known sensitivity of the used microphones M (in [V/Pa]), and the aerosol mass concentration C (in [$\mu g/m^3$]) being measured with the help of an instrument like scanning mobility particle sizer (SMPS). The PA cell constant C_{cell} (in [Pa m W^{-1}]) can be calibrated using reference gas with known concentration as described by Eq. (1). In this case, α_0 is the cross section in [m^2/molecule] of the molecule used for calibration, and C is the known concentration in [molecule/cm^3] of the involved calibration molecule:

$$C_{cell} = \frac{S - S_b}{C} \times \frac{1}{P \times M \times \alpha_0} \quad (2)$$

For this purpose, NO_2 as a good candidate with its broad absorption band in the UV–visible region was used for the determination of C_{cell} in the present work.

Fig. 4 shows the result of the PAS sensor calibration using NO_2 with known concentration that was determined using a reference NO_x analyzer (Model 42i, Thermo Scientific): PA signals versus NO_2 concentrations at atmospheric pressure.

A good linear fit of the PA signal vs. NO_2 concentration was found: $y = 0.27x + 2.88$ with a regression coefficient R = 0.999.

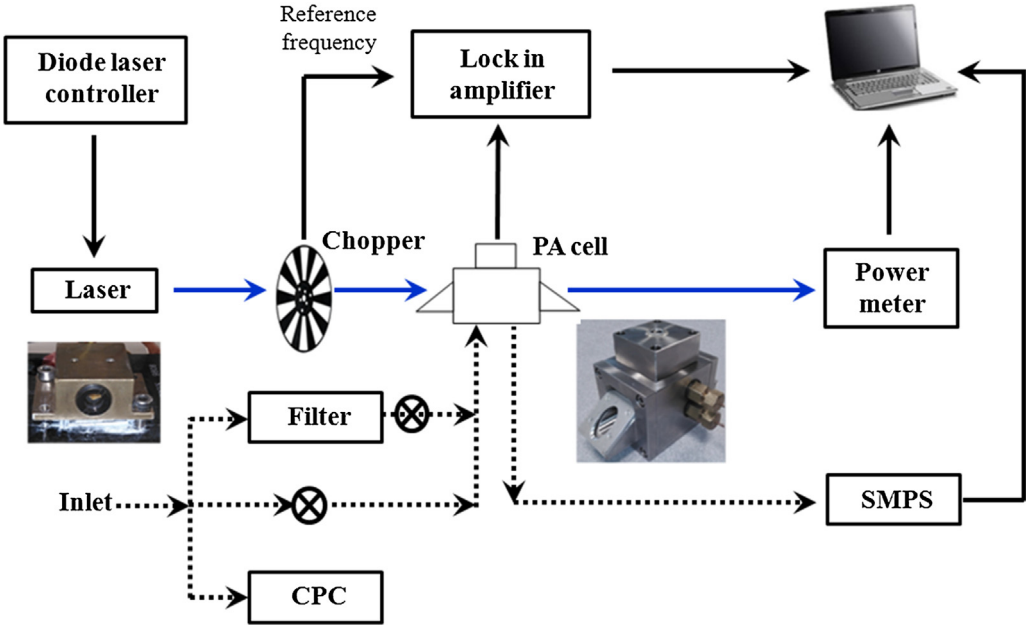

Fig. 3. Schematic of the used PA spectrophone for the measurement of black carbon absorption. CPC: concentration particle counter; SMPS: scanning mobility particle sizer.

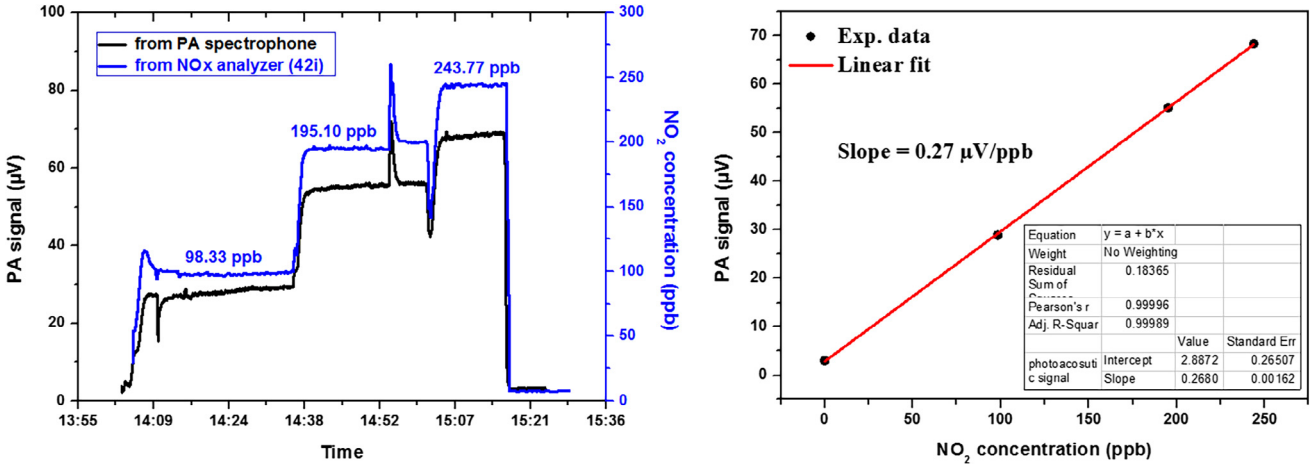

Fig. 4. *left:* PA signals vs. NO_2 concentrations. *right*: linear fit of PA signals to the NO_2 concentrations.

Given a linear slope $(S - S_b)/C = 0.27$ μV/ppb, a laser power P = 394 mW, a microphone sensitivity M = 89.6 mV/Pa and a specific absorption coefficient α_0 of 1.18 Mm^{-1}/ppb (for NO_2 at 293 K and 1 atm [20]), the PA cell constant C_{cell} was determined to be 6.48 Pa m W^{-1}.

2.3. Laboratory measurements

In order to test, characterize and validate the developed PAS sensor, measurements of reference BC in laboratory have been performed.

BC size distribution and mass concentration were simultaneously measured with a scanning mobility particle sizer (SMPS 3936, TSI) consisting of a differential mobility analyzer (DMA 3080, TSI) and a condensation particle counter (CPC 3776, TSI). The SMPS classifies the particle size ranging from 2.5 nm to 1000 nm by an electrostatic classifier. The SMPS scan up time was set to 3 min at a sample flow rate of 0.3 L/min. BC sample (graphite) measured in the experiment was from Aldrich with a density of 1.828 g/cm^3 and sizes less than 500 nm. The inlet of the PA cell was divided into two parts, one containing an aerosol filter to remove the BC for background (including atmospheric gas absorption) measurement, and another one without filter for BC (including background contribution) measurements. Time series measurements of BC absorption by the PAS sensor and its number concentration by the CPC are shown in Fig. 5 (*left*).

PA signal in [μV] vs. BC mass concentration C in [μg/m^3] measured by the SMPS is plotted in Fig. 5 (*right*) showing a good linearity with $y = 2.55x - 0.54$, which allowed one to determine mass absorption α_0 of the BC sample using Eq. (1):

$$\alpha_0(\text{in } [\text{m}^{-1}/(\mu\text{g/m}^3)]) = \frac{S - S_b}{C} \times \frac{1}{P \times M \times C_{cell}} \quad (3)$$

A mass absorption of BC was deduced to be 11.15 ± 0.83 m^2/g at 444 nm with a relative uncertainty of about 7.4%. Following the power-law, this result is in coherence with the value of 9.1 m^2/g determined at 532 nm [21]. The 1σ minimum detectable absorption coefficient of the PAS sensor is derived to be 1.18 Mm^{-1} in 1 s which corresponds to a normalized noise equivalent absorption coefficient (NNEAC) of 1.5×10^{-8} $Wcm^{-1}Hz^{-1/2}$ and a minimum measurable BC mass concentration of 0.11 μg/m^3.

In order to evaluate the potential improved performance of the developed PA spectrophone with the integration measurement time, Allan variance analysis [22] was carried out using a time series measurement of N_2 in the PA cell (black curve, upper panel in Fig. 6). From the Allan deviation plot (Fig. 6, lower panel, blue line),

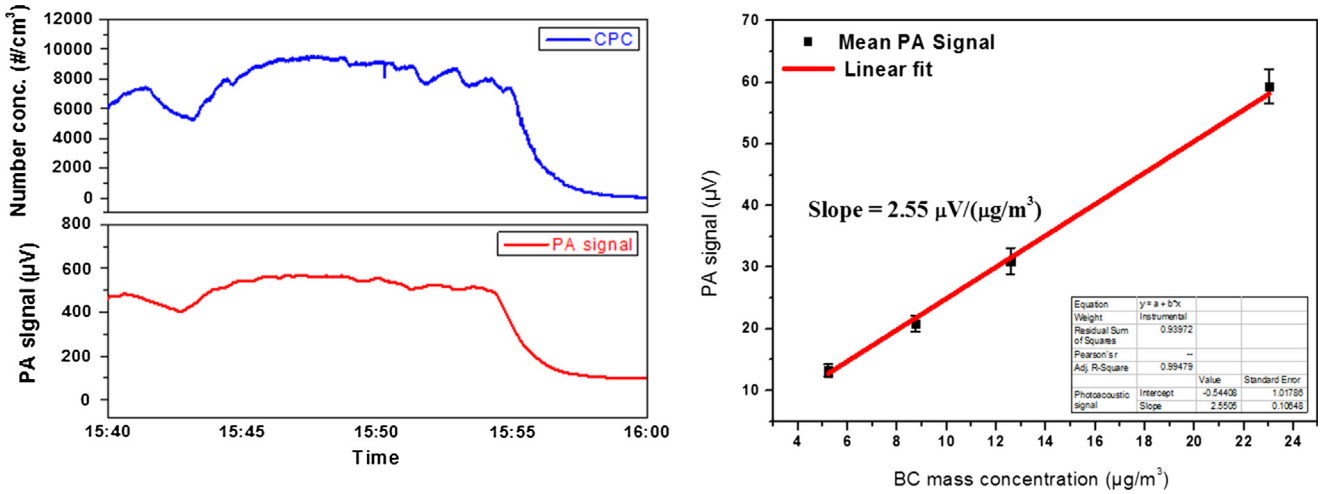

Fig. 5. *left*: time series measurements of PA signal following the variation of BC number concentration, measured by a CPC with a time solution of 1 s; *right*: fit of PA signal vs. BC mass concentration measured by a SMPS with a time solution of 135 s.

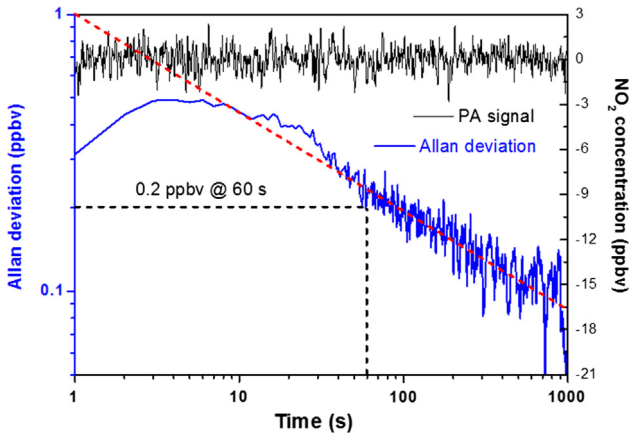

Fig. 6. Allan variance plot.

an Allan deviation of 0.2 ppbv is obtained with an integration time of 60 s, which corresponds to a min measurable volumetric mass density of 21 ng/m^3 (in 60 s) for black carbon.

Though this minimum BC detection limit value of 21 ng/m^3 is about two time higher than the SP2 value of 10 ng/m^3 [23], it is smaller than the value of 30 ng/m^3 (@ 1 min) for the filter-based aethalometer for BC [24]. It is worth noting also that the measurement uncertainties of SP2 and aethalometer are around 25% [23] and 12–30% [4], respectively, compared to that of ~7.4% for the filter-free measurement using PA spectrophone in our study. In addition, apart from the advantage of very low-cost for PA sensor (less than 1000 $), its detection limit could be further improved by using higher laser power and Kalman filtering [25]. We achieved recently a better detection limit of about 50 pptv for NO_2 which corresponds to a minimum BC detection limit of ~5 ng/m^3.

After that, the developed PA spectrophone has been applied to MAC measurement of Eyjafjallajökull volcanic ash from the 2010 eruption. The MAC of the volcanic ash has been retrieved, for the first time, from filter-free direct optical measurement of its light absorption. The result of 0.050 ± 0.002 m^2/g at 444 nm [26] was in excellent agreement, within the standard deviations, with the value derived from well controlled filter-based measurements of optical reflectance [27].

The developed PAS sensor was also applied, for the first time to our knowledge, to optical monitoring of the formation of secondary organic aerosols (SOA) produced from the photolysis of 2-nitrophenol in an atmospheric simulation chamber at University College Cork (Ireland) [26]. The objective of this study is to investigate the SOA optical properties and their impacts on the climate change.

3. Identification of CH_4 source monitored by direct absorption spectroscopy (DAS)

CH_4, one of the most important SLCPs with an atmospheric lifetime of about 12 years, is considered as one of the most powerful climate-forcing agents in the atmosphere after CO_2. A recent study revealed that the U.S. Environmental Protection Agency's (EPA) inventory of greenhouse gases (GHGs) is undercounting total U.S. CH_4 emissions by roughly 50% [28]. This study demonstrates the importance of proper data collection (ex. better measurements of ground level emissions) to find the missing methane and hence to efficiently reduce CH_4 emissions once the right sources can be targeted. Moreover, CH_4 emission from animals, rice cultivation, and energy-related sources may be prone to future increases due to demands of increasing human populations.

In the present work, we developed a quantum cascade laser (QCL)-based optical sensor for *in situ* real-time monitoring of CH_4 in the environment by direct absorption spectroscopy (DAS) in a multipass cell, with the objective of understanding and inventorying CH_4 sources.

As the absorption intensity follows an exponential law with the optical absorption length, the use of long-path absorption schemes is, apart from selection of optimum spectral absorption region, the essential way to improve the spectroscopic measurement sensitivity [29]. Long-path optical absorption can be achieved by means of multiple reflections of probing light in a high optical finesse cavity [30] or a multipass cell (MPC). MPCs are usually formed with two or more reflecting mirrors [31] with a capacity of providing typical effective optical path lengths L_{eff} ranging from 18 to 200 m (leading to ppmv-ppbv detection limits for point measurement). Since the light intensity leaking from the multipass cell reduces exponentially with the number of reflections, high reflectivity mirrors are necessary to obtain a maximum number of reflections with sufficient light exiting the cell for sensitive spectroscopic measurements. Commonly used multipass cells include: *White cells* [32], *Chernin cell* [33], *Herriott cells* [34], *Modified Herriott cell* [31] and *Dense-pattern multipass cell* [35,36].

3.1. QCL-MPC experimental setup

A typical MPC-based long-path absorption spectroscopic instrument is depicted in Fig. 7. The used continuous-wave QCL operates near 8 μm and tunable in frequency by adjusting the laser temperature and current.

In brief, a beam splitter (10–90%) was used to divide the incident QCL beam into two parts. The 10% reflected light was directed to a Fabry-Perot etalon for laser frequency metrology. The main part (90%) is directed into a White-type multipass cell (107-V Infrared Analysis, Inc.) to optically quantify CH_4 concentration by direct absorption spectroscopy. The effective optical path-length L_{eff} was about 175 m. A red laser beam, co-aligned with the mid-infrared laser beam, was used to facilitate optical beam alignment with the MPC. The emerging laser beam was focused, by means of a lens with a focal length of 50 mm, onto a thermoelectrically cooled infrared photovoltaic detector (VIGO PVI 4-TE-10.6) with a detectivity of 2×10^9 cm Hz$^{1/2}$/W and a responsivity of 0.7 A/W. The absorption signal was acquired using a high-speed digital oscilloscope (LeCroy WaveSurfer 104 MXs, Teledyne Technologies Inc.) at a sampling rate of 5 GS/s and 1 GHz bandwidth. Post processing of the recorded data was carried out to retrieve CH_4 concentration based on the Beer-Lambert law.

3.2. Retrieval of CH_4 gas concentration from direct absorption spectrum

Selection of appropriate absorption lines is crucial for spectroscopic monitoring of trace gas. A tradeoff between the required sensitivity and spectral selectivity must be usually made. Fig. 8 shows a simulated spectrum of a CH_4 absorption line centered at 1255.0004 cm^{-1} (the transition 7F2,4 ← 8F1,2 of the ν_4 fundamental band with a line intensity of 2.07×10^{-20} cm molecule^{-1}) [37]. The simulation was made with 2 ppmv CH_4 in an absorption cell with an effective optical path-length of L_{eff} = 175 m at 40 mbar. Potential interferences from ambient CO_2 (at 400 ppmv) and 1% H_2O vapor are taken into account in the simulation. As can be seen, this line is free of interference from the absorptions of CO_2 and H_2O, and was then selected for optical measurement of CH_4 concentration. Though the absorption intensity of this CH_4 absorption line is not the strongest, it is strong enough for detection of atmospheric CH_4 at its natural concentration level (~1.7 ppmv).

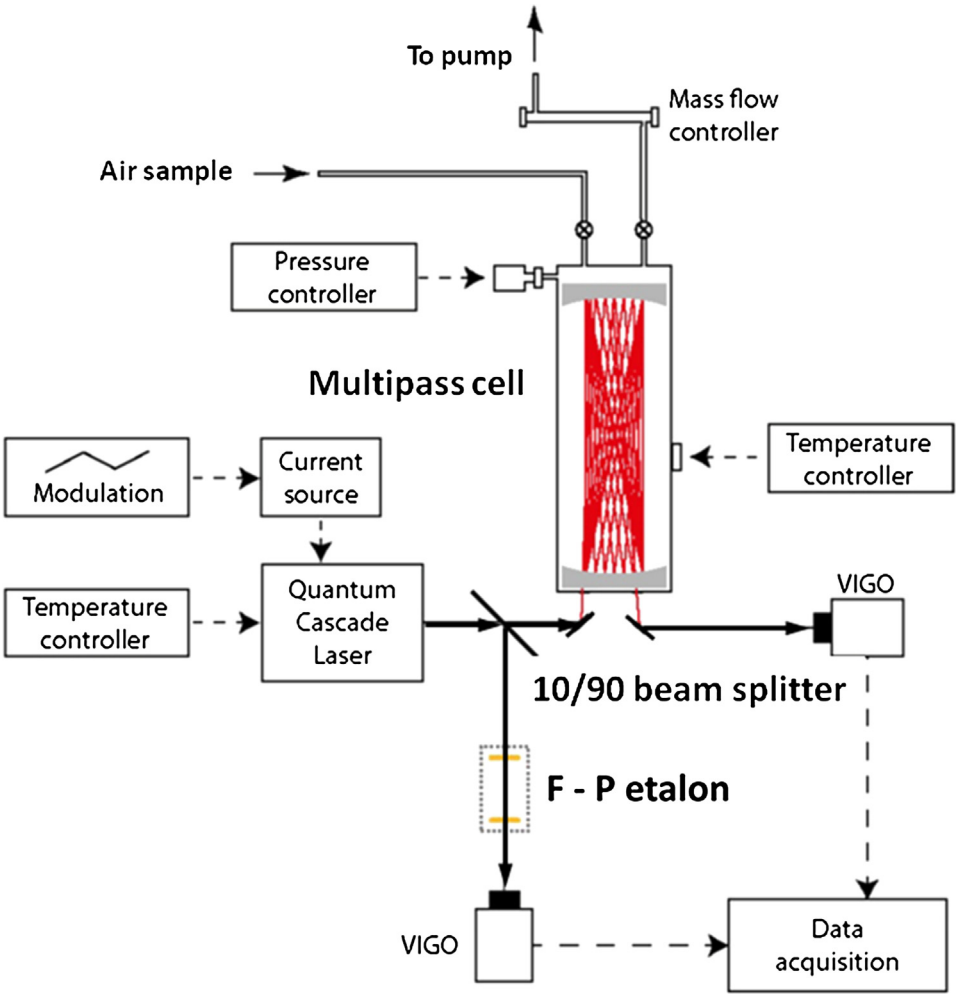

Fig. 7. QCL-based CH_4 monitor employed in the present work.

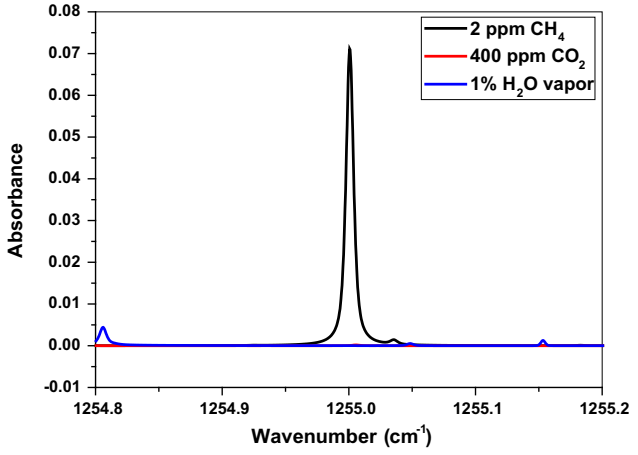

Fig. 8. Simulation of 2 ppmv CH_4 absorption spectrum around 1225 cm^{-1} in a multipass cell of 175 m optical path length at 40 mbar for interference-free monitoring of CH_4 in ambient air.

CH_4 absorption signal was recorded as a function of the acquisition data number during the scan (via laser current tuning) of the laser frequency across the target absorption line. In order to convert this absorption signal as a function of time into an absorption spectrum (as a function of frequency), interference fringes from the Fabry-Perot etalon were recorded and used to determine the relationship between the data number and the related frequency. While the absolute frequency was determined using the CH_4 absorption positions given in the HITRAN database [38].

Retrieval of trace gas concentration from the measured direct absorption spectrum is based on the Beer-Lambert law:

$$I(\nu) = I_0(\nu) \times \exp\{-C \times L \times \sigma(\nu)\} = I_0 \times \exp\{-A(\nu)\} \quad (4)$$

and

$$A(\nu) = \ln\left(\frac{I_0(\nu)}{I(\nu)}\right) = L \times C \times \sigma(\nu) \quad (5)$$

where $I_0(\nu)$ and $I(\nu)$ are the transmitted laser intensities without and with analyte in the absorption cell, respectively. L is the effective optical path-length in (cm), C is the concentration in (molecule/cm^3) of the analyte, $A(\nu)$ is the absorbance, and $\sigma(\nu)$ in (cm^2/molecule) is the frequency-dependent absorption cross section of the target analyte.

Integral absorbance A_I of the absorbance $A(\nu)$, in (cm^{-1}), over all the scanned spectral range can be written as:

$$A_I = \int A(\nu)d\nu = \int L \times C \times \sigma(\nu)d\nu \quad (6)$$

where $\int \sigma(\nu)d\nu = S$ in (cm/molecule) is the absorption line intensity.

The concentration of the target gas molecule χ_{ppm} in [ppmv] can be then determined by:

$$\chi_{ppm} = \frac{C}{N(T,P)} \times 10^6 = \frac{A_I \times P_0 \times T}{S \times L \times N_L \times P \times T_0} \times 10^6 \quad (7)$$

where N is the total molecules number per unit volume (molecules/cm^3) at pressure P and temperature T. N_L is the Loschmidt constant (=2.68678 × 10^{19} molecules/cm^3), P_0 and T_0 are the pressure and the temperature at standard conditions (1013.25 mbar and 273.15 K), respectively.

Allan variance analysis was performed to determine the performance of the developed CH_4 sensor. As can be seen in Fig. 9, the optimal data averaging time was 218 s.

Outdoor environmental air was sampled from the campaign site and drawn to the inlet of the MPC via a Teflon tube. The outlet of the cell was connected to a primary pumping system to maintain a regular sampling gas flow at a constant rate of 41.6 L/min, resulting in a gas residence time of about 36 s. Temperature and pressure of the gas sample inside the MPC were typically set at 30 °C and 42 mbar (optimized as a compromise between spectral selectivity and detection sensitivity), respectively. The temperature was controlled by using a heating jacket with a silicone-based heating blanket which was controlled by a thermocouple to heat the cell chamber uniformly. A digital temperature control unit (Infrared Analysis, Inc.) maintains temperature with a precision of ±0.01 °C.

In the present work, standard CH_4 concentration of 3000 ppmv was used at different pressures to calibrate the QCL-CH_4 sensor. The overall uncertainty on the concentration value deduced from the spectroscopic measurement was about 5.1% which was mainly related to the uncertainties in the line intensity reported in the HITRAN database (ΔS < 5%), in comparison with the uncertainties in the Voigt profile fit (~1%), in the effective optical path length L_{eff} (=0.05%), in pressure (ΔP = 0.2%) and in temperature (ΔT = 0.03%). The measurement precision was about 33.88 ppmv (corresponding to a relative uncertainty in the measurement precision of 1.13%) [38].

Fig. 10 shows a typical experimental absorption spectrum of ambient CH_4, recorded at P = 41.6 mbar and T = 303.15 K. Using a Voigt profile to fit the spectrum, the corresponding concentration of (1870 ± 16) ppb was retrieved with a 1σ detection limit of about 33.3 ppb.

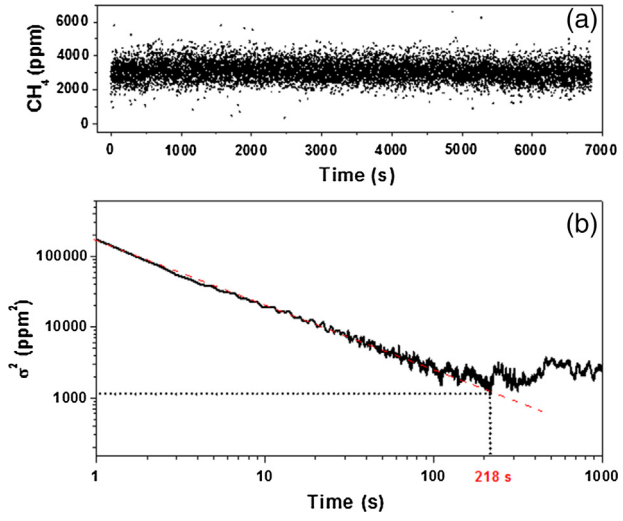

Fig. 9. (a) Time-series measurements of 3000 ppmv CH_4 data; (b) Allan deviation plot based on the 10,540 consecutive 0.65-s recorded CH_4 concentration data.

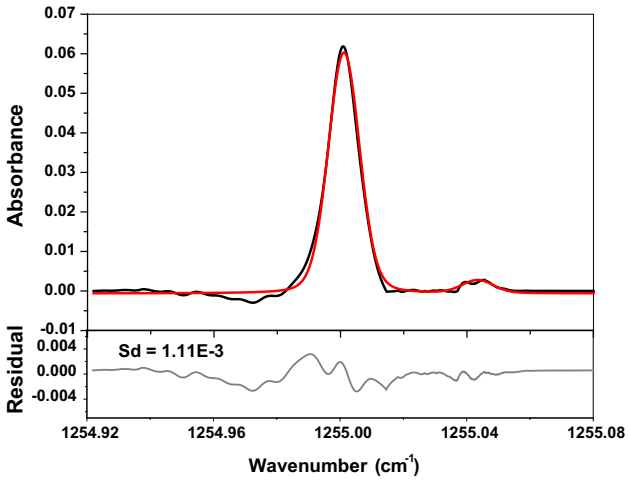

Fig. 10. *Upper panel:* Absorption spectrum of CH_4 (black curve) in ambient air and Voigt profile fit (red). *Lower panel:* Fit residual. (For interpretation of the references to colour in this figure legend, the reader is referred to the web version of this article.)

3.3. Tracing CH_4 concentration in the environment

The observation site is a suburban site in Dunkirk (France) near a moderate-traffic road (latitude/longitude: 51.0358613/2.3654160). Basic meteorological parameters (such as temperature, wind direction, wind speed, water vapor mixing ratio, global solar radiation) and major regulated gases (CO, NO_x, O_3, SO_2) were simultaneously measured. Fig. 11 shows a time series measurements of environmental CH_4 concentration (upper panel) during two weeks from 9th to 22nd January. The daily averaged CH_4 concentration >1.6 ppmv during this observation period. The occasional variation in CH_4 concentration lower than its atmospheric background may be attributed to slight offset/drift in the measurements. As can be seen, a very high CH_4 concentration of up to ~3 ppmv appeared starting from ~15:00 (Paris winter local time) on 17th January.

Based on the measured time-series concentration of NO_x, NO_2, NO, CO, SO_2 and H_2O vapor, associated with the measured meteorological parameters, this episode of high temporal variability of CH_4 has been identified and attributed to urban pollution transported by air mass through local urban area and the district of Lille. This was confirmed by the pollution wind rose of CH_4 concentrations in relation to wind sector (Fig. 12 *left*) and by the analysis of air mass back trajectories using the HYSPLIT (Hybrid Single-Particle Lagrangian Integrated Trajectory) model (Air Resources Laboratory, NOAA) [40] (Fig. 12 *right*) as well as by the analysis of the air quality monitoring data from a regional network site in Lille (Fig. 11 middle and lower panels).

A highest pollution episodes of NO_x and PM10 have been also observed on 17th January, the same day as the biggest CH_4 concentration appeared in Dunkirk. A significant increase of NO_x and PM10 levels in air (Fig. 11 middle and lower panels) was recorded at around 7:00 in Lille. As indicated by the air mass trajectory (red) in Fig. 12 (*right*) it was transport northwards and arrived in Dunkirk at around 16:00, at the moment the increasing CH_4 concentration were measured.

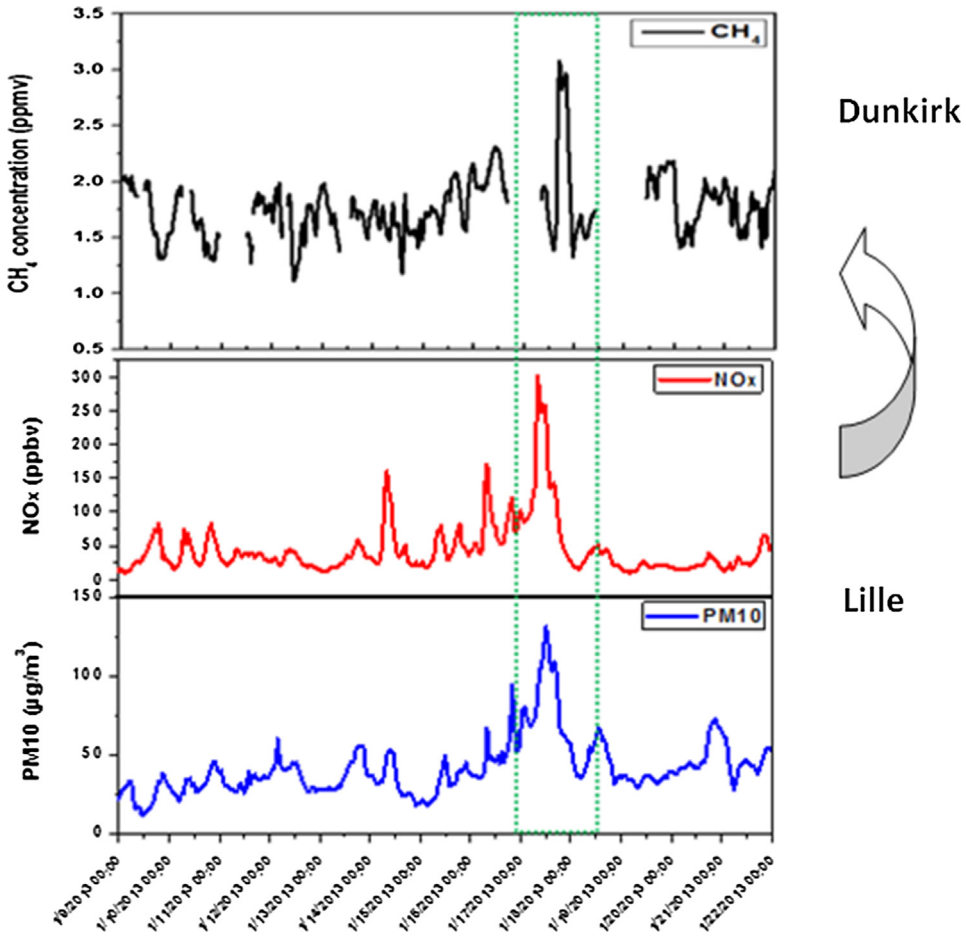

Fig. 11. Time-series CH_4 concentrations (upper panel), measured from 9th to 22nd January, associated with Lille air quality monitoring data of NO_x (middle) and PM10 (lower), recorded by the observation station of the ATMO Nord–Pas-de-Calais [39] in Lille for the same period of 9th–22nd January. A high pollution episode has been also observed on 17th January.

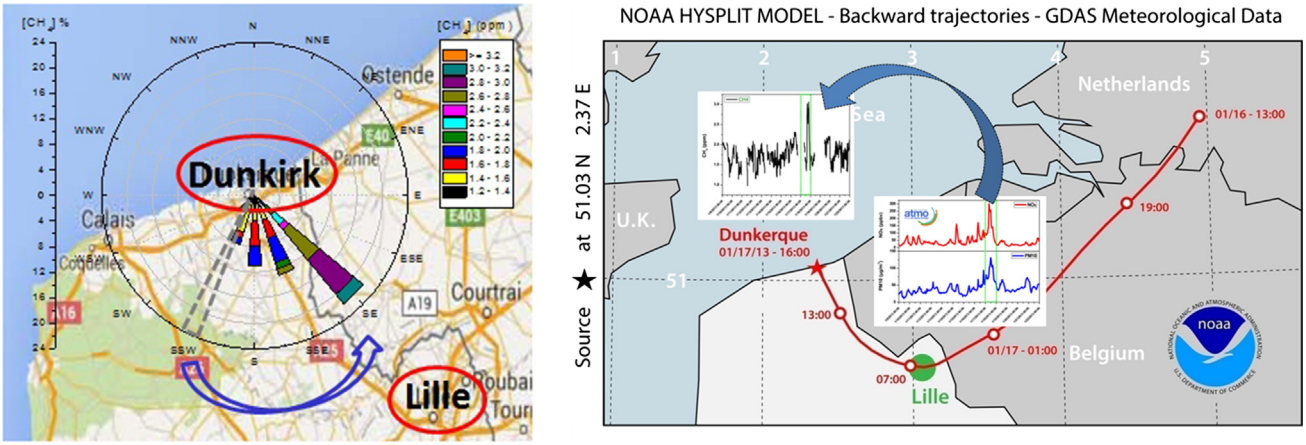

Fig. 12. *left*: Frequency distribution rose of CH_4 concentrations depending on the blowing wind sectors on 17th January; *right*: Air mass back trajectory (NOAA HYSPLIT) from Lille to Dunkirk on 17th January.

4. Conclusion

Spectroscopic measurement techniques are a powerful and versatile chemical analysis tool for identification and quantification of the presence of gaseous and particular constituents in the atmosphere [29,41]. With respect to conventionally used chemical measurement instruments (like gas chromatography, mass spectrometry, chemiluminescence, etc.), spectroscopic measurement techniques take advantage of ability to make *in situ*, real time, self-calibration, fast and absolute quantitative assessments without any sample preparation.

Since the last decade, atmospheric environmental monitoring has benefited from the development of emerging spectroscopic techniques owing to the significant breakthroughs in advanced photonic technology, including greater availability of light sources at desired wavelengths (from the UV to the mid-infrared),

high-performance photonic components, such as high reflectivity mirrors, room (or TEC) temperature operation detectors with fast time response and shot-noise-limited sensitivity, etc. There is ongoing demand for highly sensitive, direct and absolute techniques for atmospheric species measurement in ground-based and airborne/UAV (unmanned aerial vehicle) field campaigns, as well as in atmospheric simulation experiments. Newly emerging and promising photonic measurement techniques (such as dual-comb spectroscopy, laser heterodyne radiometry, etc.) [42] will continue to mature and provide new and improved instrumentation suitable for fast, accurate and precise measurements for a wide range of laboratory and field applications. Examples include the studies of missing source of HONO [43,44], missing OH reactivity [45,46], missing oxidant [47], etc.

Apart from the continuous improvement of the instrument performance for concentration measurements, the future work would include developing spectroscopic methods to measure vertical concentration profiles and flux (to study budgets, variability and trends) of key atmospheric species, and isotopic composition analysis (to study the origin, evolution and dispersion of these chemical species in the atmosphere). All of them will help us to improve our understanding of tropospheric processes for prediction of future changes in atmospheric composition, and to develop strategies for mitigation of climatic impacts from non-CO_2 greenhouse gases and aerosols.

Acknowledgments

This work is supported by the French national research agency (ANR) under the CaPPA (ANR-10-LABX-005) and the MABCaM (ANR-16-CE04-0009) contracts. The authors thank the financial support from the CPER-CLIMIBIO program, the funding from the French embassy in Ireland and from the communauté d'Universités et d'Etablissements Lille Nord de France, and from the BQI program of the Université du Littoral Côte d'Opale.

References

[1] G.R. Sonnemann, M. Grygalashvyly, Effective CO_2 lifetime and future CO_2 levels based on fit function, Ann. Geophys. 31 (2013) 1591–1596.
[2] D. Zaelke, Primer on Short-Lived Climate Pollutants, IGSD (23 April 2013).
[3] IPCC report (2013). <http://www.ipcc.ch/report/ar5/wg1/>.
[4] D.A. Lack, H. Moosmüller, G.R. McMeeking, R.K. Chakrabarty, D. Baumgardner, Characterizing elemental, equivalent black, and refractory black carbon aerosol particles: a review of techniques, their limitations and uncertainties, Anal. Bioanal. Chem. 406 (2014) 99–122.
[5] T.C. Bond, S.J. Doherty, D.W. Fahey, P.M. Forster, J. Berntsen, T.B. DeAngelo, M. G. Flanner, S. Ghan, B. Kärcher, D. Koch, S. Kinne, Y. Kondo, P.K. Quinn, M.C. Sarofim, M.G. Schultz, M. Schulz, C. Venkataraman, H. Zhang, S. Zhang, N. Bellouin, S.K. Guttikunda, P.K. Hopke, M.Z. Jacobson, J.W. Kaiser, Z. Klimont, U. Lohmann, J.P. Schwarz, D. Shindell, T. Storelvmo, Bounding the role of black carbon in the climate system: a scientific assessment, J. Geophys. Res.: Atmos. 118 (2013) 5380–5552.
[6] J.E. Hansen, M. Sato, Trends of measured climate forcing agents, PNAS 98 (2001) 14778–14783.
[7] M.O. Andreae, A. Gelencer, Black carbon or brown carbon? The nature of light-absorbing carbonaceous aerosols, Atmos. Chem. Phys. 6 (2006) 313–3148.
[8] O. Schmid, P. Artaxo, W.P. Arnott, D. Chand, L.V. Gatti, G.P. Frank, A. Hoffer, M. Schnaiter, M.O. Andreae, Spectral light absorption by ambient aerosols influenced by biomass burning in the Amazon Basin I: comparison and field calibration of absorption measurement techniques, Atmos. Chem. Phys. 6 (2006) 3443–3462.
[9] Review of evidence on health aspects of air pollution – REVIHAAP, Technical Report, World Health Organization, 2013.
[10] A.L. Daniel, R.L. Edward, B. Tahllee, P. Anders, A.R. Ravishankara, Aerosol absorption measurement using photoacoustic spectroscopy: sensitivity, calibration, and uncertainty developments, Aerosol Sci. Technol. 40 (2006) 697–708.
[11] A.L. Daniel, S.R. Mathews, L. Daniel, M.L. Justin, D.C. Christopher, J.M. Richard, M.M. Daniel, Aircraft instrument for comprehensive characterization of aerosol optical properties, Part 2: black and brown carbon absorption and absorption enhancement measured with photo acoustic spectroscopy, Aerosol Sci. Technol. 46 (2012) 555–568.
[12] R.W. Joseph, L.D. Mathews, D.S. Geoffrey, A UV-vis photoacoustic spectrophotometer, Anal. Chem. 86 (2014) 6049–6056.
[13] F.J.M. Harren, G. Cotti, J. Oomens, S.L. Hekkert, Photoacoustic spectroscopy in trace gas monitoring, in: R.A. Meyers (Ed.), Encyclopedia of Analytical Chemistry, Wiley, 2000, pp. 2203–2226.
[14] Z. Bozoki, A. Mohacsi, G. Szabo, Z. Bor, M. Erdelyi, W. Chen, F.K. Tittel, Near infrared diode laser based spectroscopic detection of ammonia: a comparative study of photoacoustic and direct optical absorption methods, Appl. Spectrosc. 56 (2002) 715–719.
[15] J. Kauppinen, K. Wilcken, I. Kauppinen, V. Koskinen, High sensitivity in gas analysis with photoacoustic detection, Microchem. J. 76 (2004) 151–159.
[16] A.A. Kosterev, Y.A. Bakhirkin, R.F. Curl, F.K. Tittel, Quartz-enhanced photoacoustic spectroscopy, Opt. Lett. 27 (2002) 1902–1904.
[17] K. Liu, X. Guo, H. Yi, W. Chen, W. Zhang, X. Gao, Off-beam quartz enhanced photoacoustic spectroscopy, Opt. Lett. 34 (2009) 1594–1596.
[18] T. Kuusela, J. Kauppinen, Photoacoustic gas analysis using interferometric cantilever microphone, Appl. Spectrosc. Rev. 42 (2007) 443–474.
[19] R.J. Pryputniewicz, Current trends and future directions in MEMS, Exp. Mech. 52 (2012) 289–303.
[20] S. Voigt, J. Orphal, J.P. Burrow, The temperature and pressure dependence of the absorption cross-sections of NO_2 in the 250–800 nm region measured by Fourier-transform spectroscopy, J. Photochem. Photobiol. A: Chem. 149 (2002) 1–7.
[21] T. Ajtai, Á. Filepm, G. Kecskemétim, B. Hopp, Z. Bozóki, G. Szabó, Wavelength dependent mass-specific optical absorption coefficients of laser generated coal aerosols determinedfrom multi-wavelength photoacoustic measurements, Appl. Phys. A 103 (2011) 1165–1172.
[22] P. Werle, R. Mücke, F. Slemr, The limits of signal averaging in atmospheric trace-gas monitoring by tunable diode-laser absorption spectroscopy (TDLAS), Appl. Phys. B 57 (1993) 131–139.
[23] A.J. Sedlacek, Single-Particle Soot Photometer (SP2) Instrument Handbook, DOE/SC-ARM-TR-169, February 2017.
[24] Benchmark Monitoring, Advanced Measurement of Black Carbon, MAGEE Scientific.
[25] T. Wu, W. Chen, E. Kerstel, E. Fertein, X. Gao, J. Koeth, K. Rößner, D. Brückner, Kalman filtering real-time measurements of H_2O isotopologue ratios by laser absorption spectroscopy at 2.73 μm, Opt. Lett. 35 (2010) 634–636.
[26] Gaoxuan Wang, Development of photonic instruments for measurement of Aerosol optical properties, PhD thesis, Université du Littoral Côte d'Opale, 2018.
[27] A. Rocha-Lima, J.V. Martins, L.A. Remer, N.A. Krotkov, M.H. Tabacniks, Y. Ben-Ami, P. Artaxo, Optical, microphysical and compositional properties of the Eyjafjallajökull volcanic ash, Atmos. Chem. Phys. 14 (2014) 10649–10661.
[28] S.M. Miller, S.C. Wofsy, A.M. Michalak, E.A. Kort, A.E. Andrews, S.C. Biraud, E.J. Dlugokencky, J. Eluszkiewicz, M.L. Fischer, G. Janssens-Maenhout, B.R. Miller, J. B. Miller, S.A. Montzka, T. Nehrkorn, C. Sweeney, Anthropogenic emissions of methane in the United States, PNAS 110 (2013) 20018–20022.
[29] F.K. Tittel, D. Richter, A. Fried, Mid-infrared laser applications in spectroscopy, in: I.T. Sorokina, K.L. Vodopyanov (Eds.), Solid-State Mid-Infrared Laser Sources, Springer-Verlag, 2003, pp. 445–510.
[30] D. Romanini, I. Ventrillard, G. Méjean, J. Morville, E. Kerstel, Introduction to cavity enhanced absorption spectroscopy, in: G. Gagliardi, H.-P. Loock (Eds.), Cavity-Enhanced Spectroscopy and Sensing, Springer, 2014, pp. 1–60.
[31] J.B. McManus, P.L. Kebabian, M.S. Zahniser, Astigmatic mirror multipass absorption cells for long-path-length spectroscopy, Appl. Opt. 34 (1995) 3336–3348.
[32] J.U. White, Long optical paths of large aperture, J. Opt. Soc. Am. 32 (1942) 285–288.
[33] S.M. Chernin, E.G. Barskaya, Optical multipass matrix systems, Appl. Opt. 30 (1991) 51–58.
[34] D. Herriott, H. Kogelnik, R. Kompfner, Off-axis paths in spherical mirror interferometers, Appl. Opt. 3 (1964) 523–526.
[35] K. Krzempek, M. Jahjah, R. Lewicki, P. Stefanski, S. So, D. Thomazy, F.K. Tittel, CW-DFB RT diode laser-based sensor for trace-gas detection of ethane using a novel compact multipass gas absorption cell, Appl. Phys. B 112 (2013) 461–465.
[36] K. Liu, L. Wang, T. Tan, G. Wang, W. Zhang, W. Chen, X. Gao, Highly sensitive detection of methane by near-infrared laserabsorption spectroscopy using a compact dense-pattern multipass cell, Sens. Actuat., B 220 (2015) 1000–1005.
[37] L.S. Rothman, D. Jacquemart, A. Barbe, D.C. Benner, M. Birk, L.R. Brown, M.R. Carleer, C. Chackerian, K. Chance, L.H. Coudert, et al., The HITRAN 2004 molecular spectroscopic database, J. Quant. Spectrosc. Radiat. Transf. 96 (2005) 139–204.
[38] R. Maamary, X. Cui, E. Fertein, P. Augustin, M. Fourmentin, D. Dewaele, F. Cazier, L. Guinet, W. Chen, Quantum cascade laser-based optical sensor for continuous monitoring of environmental methane in dunkirk (France), Sensors 16 (2016) 224.
[39] ATMO Nord–Pas-de-Calais. Available online: <http://www.atmo-npdc.fr/> (accessed on 25 January 2016).
[40] R.R. Draxler, G.D. Rolph, HYSPLIT (HYbrid Single-Particle Lagrangian Integrated Trajectory). NOAA Air Resources Laboratory, College Park, MD, USA. Available online: <http://www.arl.noaa.gov/HYSPLIT.php> (accessed on 11 December 2015).
[41] M.W. Sigrist (Ed.), Air Monitoring by Spectroscopic Techniques, John Wiley & Sons Inc., New York, 1994.

[42] W. Chen, H. Yi, T. Wu, W. Zhao, C. Lengignon, G. Wang, E. Fertein, C. Coeur, G. Wysocki, T. Wang, M.W. Sigrist, X. Gao, W. Zhang, Photonic sensing of reactive atmospheric species, in: R.A. Meyers (Eds.), Encyclopedia of Analytical Chemistry, © 2017, John Wiley & Sons, Ltd. doi: 10.1002/9780470027318.a9432.

[43] H. Su, Y. Cheng, R. Oswald, T. Behrendt, I. Trebs, F.X. Meixner, M.O. Andreae, P. Cheng, Y. Zhang, U. Pöschl, Soil nitrite as a source of atmospheric HONO and OH radicals, Science 333 (2011) 1616–1618.

[44] L. Zhang, T. Wang, Q. Zhang, J. Zheng, Z. Xu, M. Lv, Potential sources of nitrous acid (HONO) and their impacts on ozone: a WRF – Chem study in a polluted subtropical region, J. Geophys. Res. Atmos. 121 (2016) 3645–3662.

[45] P. Di Carlo, W.H. Brune, M. Martinez, H. Harder, R. Lesher, X. Ren, T. Thornberry, M.A. Carroll, V. Young, P.B. Shepson, D. Riemer, E. Apel, C. Campbell, Missing OH reactivity in a forest: evidence for unknown reactive biogenic VOCs, Science 304 (2004) 722–725.

[46] A.C. Nolscher, A.M. Yanez-Serrano, S. Wolff, A. Carioca de Araujo, J.V. Lavric, J. Kesselmeier, J. Williams, Unexpected seasonality in quantity and composition of Amazon rainforest air reactivity, Nat. Commun. 7 (2016) 10383.

[47] C. Reed, M.J. Evans, P. Di Carlo, J.D. Lee, L.J. Carpenter, Interferences in photolytic NO_2 measurements: explanation for an apparent missing oxidant?, Atmos Chem. Phys. 16 (2016) 4707–4724.